Article

New PKS/NRPS Tenuazamines A–H from the Endophytic Fungus *Alternaria alternata* FL7 Isolated from *Huperzia serrata*

Hao Zhang [1], Zhibin Zhang [2], Yiwen Xiao [1,2,*], Wen Wang [1], Boliang Gao [1], Yuhao Xie [1], Jiahao Xie [1], Xinhua Gao [1] and Du Zhu [1,2,*]

[1] Jiangxi Province Key Laboratory of Natural Microbial Medicine Research, Key Laboratory of Microbial Resources and Metabolism of Nanchang City, College of Life Sciences, Jiangxi Science and Technology Normal University, Nanchang 330013, China; 17609234825@163.com (H.Z.); wenwang_jiangxi@163.com (W.W.); gaoboliangspinach@aliyun.com (B.G.); hao18295767732@163.com (Y.X.); xiejiahao20010202@163.com (J.X.); gaoxinhuade@126.com (X.G.)

[2] Jiangxi Province Key Laboratory of Biodiversity Conservation and Bioresource Utilization, School of Life Sciences, Jiangxi Normal University, Nanchang 330022, China; zzbbio@jxnu.edu.cn

* Correspondence: xyw1152858687@163.com (Y.X.); zhudu12@163.com (D.Z.)

Abstract: In this paper, we present a novel class of hybrid polyketides, tenuazamines A–H (**1–8**), which exhibit a unique tautomeric equilibrium from *Alternaria alternata* FL7. The elucidation of the structures was achieved through a diverse combination of NMR, HR-ESIMS, and ECD methods, with a focus on extensive spectroscopic data analysis. Notably, compounds **1**, **4**, **8–9** exhibited potent toxic effects on the growth of *Arabidopsis thaliana*. This research expands the structural diversity of tenuazonic acid compounds derived from endophytic fungi and provides potential hit compounds for the development of herbicides.

Keywords: *Alternaria alternata*; *Huperzia serrata*; tenuazamine; tautomer; herbicides

1. Introduction

The genus *Alternaria alternata* (Fr.) Keissl., a member of the family *Pleosporaceae*, is known to exist as an endophyte, a parasite, or a saprophyte in various environments [1], such as soil, plants, air, and even some insects' bodies [2–5]. *A. alternata* has been identified as a source of tenuazonic acid compounds (TeAs), alternariol (AOH), alternariol monomethyl ether (AME), altenuene (ALT), and tentoxin (TEN) [6]. Among these natural products, TeAs characterized by a pyrrolidine-2, 4-dione ring, are the most toxic (Figure S1, Supporting Information, SI) [7].

Tenuazonic acid (TeA, **9**, Figure S1, Supporting Information, SI) was first isolated in 1957 from the cultures of *A. tenuis* [8]. TeAs have been reported to be produced in other plant pathogenic fungi, such as *Ageratina adenophora*, *Stemphylium loti*, and *Epicoccum sorghinum* [9–11], with a broad spectrum of biological activities, including antitumor (TeA, **9**, Figure S1, Supporting Information, SI) [12], antifungal (cladodionen, **23**, Figure S1, Supporting Information, SI) [13], antiviral (cladosins C, **24**, Figure S1, Supporting Information, SI) [14], antibacterial and antibiotic (paecilosetin **16**, and altersetin **17**, Figure S1, Supporting Information, SI) [15,16], insecticidal, and phytotoxic activities (trichosetin, **27**, Figure S1, Supporting Information, SI) [17,18].

To the best of our knowledge, there are few reports about tautomer on the related secondary metabolites of *A. alternata* from endophytic fungus [19]. In this study, we considerably enriched the structural diversity of secondary metabolites of *A. alternata* and systematically determined its phytotoxicity in model plant, *Arabidopsis thaliana* (L.) Heynh. and providing potentially active compounds for eco-friendly weed control applications.

2. Materials and Methods

2.1. General Experimental Procedures

Electronic circular dichroism (ECD) spectra were measured using a Chirascan spectropolarimeter (Applied Photophysics, Leatherhead, UK). Column chromatography was performed using a 200–300-mesh silica gel (Qingdao Marine Chemical Co., Ltd., Qingdao, Shandong, China), a reversed-phase C18 gel (YMC Co., Ltd., Kyoto, Japan), and Sephadex LH-20 (GE Healthcare, Chicago, IL, USA). Semipreparative reversed-phase HPLC was performed using a Waters system (Milford, MA, USA) comprising a 2535 quaternary pump and a 2996 controller coupled to a 2489 dual-absorbance detector. UPLC-QToF-HRMS analyses were performed on ACQUITY H-Class UPLC (Waters system) coupled to a Xevo® G2-XS Q-TOF instrument (Waters system) with an ESI interface. All NMR spectra were acquired using an AVNEO 400-MHz NMR spectrometer (Bruker, Billerica, MA, USA). UV–vis spectroscopy was performed using a Lambda 365 instrument (PerkinElmer, Waltham, MA, USA). *Arabidospsis thaliana* was purchased from Zhengzhou Arabidopsis Biotechnology Co., Ltd. (Zhengzhou, Henan, China).

2.2. Molecular Identification of the Endophytic Fungi

The endophytic fungus FL7 was isolated from *H. serrata* at the Lushan Botanical Garden in Jiangxi Province and the Chinese Academy of Sciences [20]. The fungal DNA extraction and amplification were performed at the Jiangxi Province Key Laboratory of Natural Microbial Medicine Research using an F917891 Fungi Genomic Fungal DNA Kit (Macklin, Shanghai, China) and the PCR conditions as previously described (in 2019) [21]. Sequencing procedures were performed at the Shanghai Shenggong Bioengineering Technology Service Co., Ltd. (Shanghai, China). Molecular identification of the fungal endophyte was performed using (i) the primer pair ITS1 (5′-TCCGTAGGTGAACCTGCGG-3′) and ITS4 (5′-TCCTCCGCTTATTGATATATGC-3′) to amplify the 5.8S region of the ribosomal DNA and the two internal spacers ITS1 and ITS2 [22]. The sequence was subjected to the pairwise comparison using the BLASTN search tool with the Megablast algorithm on the NCBI platform. Top matching sequences were obtained considering similarity levels for species identification of 99.65% [21]. Therefore, it was identified as *A. alternata*. It was stored at the China Typical Culture Collection Center (http://cctcc.whu.edu.cn/) accesed on 24 October 2022 under the collection number CCTCC M 2023428.

2.3. Fermentation and Extraction

The endophytic fungus FL7 stored in an ultralow-temperature refrigerator at −80 °C was thawed, inoculated into Petri dishes containing PDA, and incubated for 7 d at 28 °C. Subsequently, mycelial hyphae were collected using an inoculation loop, transferred to Erlenmeyer flasks containing PDB, and shaken at 28 °C and 180 rpm/min for 4 d to prepare the seed solution. FL7 was inoculated in a solid brown rice medium in 500×1 L Erlenmeyer flasks, each containing 80 g of brown rice and 120 mL of tap water, and sterilized at 121 °C for 21 min in an autoclave.

After incubation at 28 °C for 30 days, the fermented material was extracted with MeOH (11 times, each for 24 h), and the solution was evaporated to dryness under reduced pressure to obtain an extract weighing 1.25 kg. The MeOH extract was mixed with an equal volume of distilled water to form a partial suspension and extracted thrice with an equal volume of petroleum ether and ethyl acetate (EtOAc) to obtain petroleum ether and ethyl acetate extracts (191 g). The EtOAc fraction was subjected to silica gel-based column chromatography with a stepwise-gradient elution using petroleum ether, petroleum-EtOAc, and EtOAc to yield four fractions 1–4. Fraction 4 (38 g) was further subjected to an MCI open-column chromatography using MeOH:H_2O in a 5:95–100:0 gradient to obtain eight subfractions 4.1–4.8. Subfraction 4.3 (8.5 g) was subjected to silica gel-based column chromatography with a stepwise-gradient elution using CH_2Cl_2:MeOH to yield six super subfractions 4.3.1–4.3.6.

Super subfraction 4.3.1 (210 mg) was purified via semipreparative RP-HPLC using 35% (*v/v*) MeOH in H_2O to afford **2** (17.5 mg; t_R = 9.2 min), **7** (1.1 mg; t_R = 13.0 min), **5** (11.4 mg; t_R = 15.0 min), and **1** (59.5 mg; t_R = 23.0 min). Super subfraction 4.3.2 (104 mg) was purified via semipreparative RP-HPLC using 10% MeOH in H_2O to afford **3** (17.9 mg; t_R = 8.0 min), **4** (34.7 mg; t_R = 10.3 min), and **6** (2.8 mg, t_R = 14.0 min). Compound **8** was precipitated from the methanol solution of super subfraction 4.3.5 and obtained via recrystallization. Super subfraction 4.3.6 (145 mg) was purified through semipreparative RP-HPLC using 70% MeOH in H_2O to afford **9** (41.2 mg; t_R = 9.1 min) and **10** (6.4 mg, t_R = 18.1 min).

Tenuazamine A (**1**): brown oil droplets; ^1H and ^{13}C data, Tables 1 and 2; UV (500 µg/mL, MeOH) λmax (logε) 291.0 nm, Figure S7; HRESIMS *m/z* 197.1290 [M+H]$^+$, (calcd. for $C_{10}H_{17}N_2O_2$, 197.1297); $[\alpha]_D^{25}$ −0.3 (*c* 2.0, MeOH).

Tenuazamine B (**2**): brown oil droplets; ^1H and ^{13}C data, Tables 1 and 2; UV (500 µg/mL, MeOH) λ_{max} 298.1 nm and 302.1 nm, Figure S14; HRESIMS *m/z* 263.1359 [M+Na]$^+$, (calcd. for $C_{12}H_{20}N_2O_3Na$, 263.1372); $[\alpha]_D^{25}$ −5.4 (*c* 1.0, MeOH).

Tenuazamine C (**3**): brown oil droplets; ^1H and ^{13}C data, Tables 1 and 2; UV (500 µg/mL, MeOH) λ_{max} 304.1 nm, Figure S21; HRESIMS *m/z* 381.1633 [M+Na]$^+$, (calcd. for $C_{16}H_{26}N_2O_7Na$, 381.1638); $[\alpha]_D^{25}$ 2.4 (*c* 1.0, MeOH).

Tenuazamine D (**4**): brown oil droplets; ^1H and ^{13}C data, Tables 1 and 2; UV (500 µg/mL, MeOH) λ_{max} 302.9 nm, Figure S28; HRESIMS *m/z* 297.1802 [M+H]$^+$, (calcd. for $C_{15}H_{25}N_2O_4$, 297.1814); $[\alpha]_D^{25}$ 0.25 (*c* 2.0, MeOH).

Tenuazamine E (**5**): brown oil droplets; ^1H and ^{13}C data, Tables 2 and 3; UV (500 µg/mL, MeOH) λ_{max} 287.4 nm, Figure S35; HRESIMS *m/z* 211.1092 [M−H]$^-$, (calcd. for $C_{10}H_{15}N_2O_3$, 211.1083); $[\alpha]_D^{25}$ 5.9 (*c* 1.0, MeOH).

Table 1. ^1H NMR Spectroscopic Data for Compounds **1–4** in DMSO-d_6.

No.	1a	1b	2a	2b	3a	3b	4a	4b
5	3.44 (1H, br d, 2.9)	3.53 (1H, br d, 2.9)	3.44 (1H, br d, 2.9)	3.52 (1H, overlapped)	3.51 (1H, br d, 2.9)	3.60 (1H, br d, 3.2)	3.41 (1H, overlapped)	3.49 (1H, br d, 3.2)
7	2.30 (3H, s)	2.33 (3H, s)	2.45 (3H, s)	2.47 (3H, s)	2.52 (3H, s)	2.57 (3H, s)	2.37 (3H, s)	2.40 (3H, s)
8	1.72 (1H, m)	1.72 (1H, m)	1.72 (1H, m)	1.72 (1H, m)	1.74 (1H, m)	1.74 (1H, m)	1.72 (1H, m)	1.72 (1H, m)
9	1.08, 1.23 (each 1H, m)	1.08, 1.23 (each 1H, m)	1.05, 1.21 (each 1H, m)	1.05, 1.21 (each 1H, m)	1.09, 1.23 (each 1H, m)	1.09, 1.23 (each 1H, m)	1.08, 1.24 (each 1H, m)	1.08, 1.24 (each 1H, m)
10	0.79 (3H, t, 7.4)	0.79 (3H, t, 7.4)	0.77 (3H, t, 7.4)	0.78 (3H, t, 7.4)	0.80 (3H, t, 7.4)	0.80 (3H, t, 7.4)	0.80 (3H, t, 7.4) [a]	0.79 (3H, t, 7.4) [a]
11	0.88 (3H, d, 7.0)	0.87 (3H, d, 6.9)	0.87 (3H, d, 7.0)	0.86 (3H, d, 6.9)	0.89 (3H, d, 6.9)	0.88 (3H, d, 6.9)	0.89 (3H, d, 6.9)	0.88 (3H, d, 6.9)
1′			3.40 (2H, m)	3.40 (2H, m)	4.69 (1H, dd, 8.7, 8.1)	4.75 (1H, dd, 8.8, 7.9)		
2′			3.55 (2H, m)	3.55 (2H, m)	3.07 (1H, t-like, 8.8)	3.08 (1H, t-like, 8.8)	3.76 (1H, dd, 9.0, 4.4)	3.82 (1H, dd, 9.0, 4.2)
3′					3.25 (1H, t-like, 9.0)	3.26 (1H, t-like, 9.0)	2.15 (1H, m)	2.13 (1H, m)
4′					3.09 (1H, t-like, 9.5)	3.09 (1H, t-like, 9.5)	0.86 (1H, d, 6.6)	0.86 (1H, d, 6.6)
5′					3.27 (1H, m)	3.27 (1H, m)	0.91 (1H, d, 6.6)	0.91 (1H, d, 6.6)
6′					3.42, 3.66 (each 1H, m)	3.42, 3.66 (each 1H, m)		
1-NH	7.53 (1H, br s)	7.31 (1H, br s)	7.55 (1H, br s)	7.29 (1H, br s)	7.84 (1H, s)	7.55 (1H, s)	7.46 (1H, s)	7.22 (1H, s)
12-NH			10.58 (1H, t, 5.7)	10.89 (1H, t, 5.6)	10.73 (1H, d, 8.1)	10.91 (1H, d, 7.9)	10.80 (1H, d, 9.0)	11.12 (1H, d, 9.0)
NH$_2$	8.64, 9.42 (each 1H, br s)	8.78, 9.67 (each 1H, br s)						

[a] Interchangeable.

Table 2. ^{13}C NMR Spectroscopic Data for Compounds **1–8** in DMSO-d_6.

No.	1a	1b	2a	2b	3a	3b	4a	4b	5a1–2	5b1–2	6a	6b	7a	7b	8a	8b
2	174.6 (s)	172.1 (s)	175.5 (s)	172.6 (s)	174.4 (s)	171.3 (s)	175.5 (s)	172.7 (s)	173.8/173.9 (s)	171.1/171.2 (s)	174.7 (s)	172.2 (s)	174.7 (s)	172.2 (s)	175.3 (s)	172.0 (s)
3	95.4 (s)	97.0 (s)	95.3 (s)	97.1 (s)	96.6 (s)	98.2 (s)	94.7 (s)	96.5 (s)	93.5/93.6 (s)	95.1/95.2 (s)	94.9 (s)	96.5 (s)	95.2 (s)	96.8 (s)	95.0 (s)	97.0 (s)
4	195.9 (s)	198.5 (s)	195.7 (s)	198.5 (s)	196.2 (s)	199.4 (s)	194.9 (s)	197.5 (s)	196.3/196.4 (s)	198.6/198.7 (s)	196.0 (s)	198.6 (s)	195.8 (s)	198.4 (s)	195.2 (s)	198.3 (s)
5	64.9 (d)	63.6 (d)	65.2 (d)	63.3 (d)	65.0 (d)	63.1 (d)	64.8 (d)	63.0 (d)	87.9/87.9 (s)	87.0/87.0 (s)	62.5 (d)	61.3 (d)	65.1 (d)	63.9 (d)	64.9 (d)	63.0 (d)
6	167.2 (s)	167.3 (s)	167.9 (s)	168.1 (s)	167.7 (s)	168.0 (s)	166.0 (s)	165.6 (s)	166.8 (s)	166.9/167.0 (s)	167.4 (s)	167.4 (s)	167.3 (s)	167.4 (s)	167.3 (s)	167.6 (s)
7	18.5 (q)	17.6 (q)	13.9 (q)	13.2 (q)	13.5 (q)	12.7 (q)	13.9 (q)	13.1 (q)	18.4/18.4 (q)	17.7/17.7 (q)	18.5 (q)	17.6 (q)	18.5 (q)	17.6 (q)	13.3 (q)	12.5 (q)
8	36.5 (d)	36.6 (d)	36.7 (d)	36.8 (d)	36.5 (d)	36.6 (d)	36.5 (d)	36.6 (d)	*	*	41.3 (d)	41.2 (d)	29.5 (d)	29.6 (d)	36.5 (d)	36.6 (d)
9	23.0 (t)	23.3 (t)	23.1 (t)	23.4 (t)	23.0 (t)	23.3 (t)	22.9 (t)	23.2 (t)	21.5/23.3 (t)	21.6/23.4 (t)	68.5 (d)	68.4 (d)	19.5 (q)	19.2 (q)	22.9 (t)	23.2 (t)
10	11.9 (q)	11.9 (q)	12.2 (q)	12.1 (q)	11.9 (q)	11.8 (q)	11.9 (q)	11.9 (q)	11.9/12.2 (q)	11.9/12.2 (q)	21.5 (q)	21.5 (q)	15.6 (q)	15.8 (q)	11.9 (q)	11.8 (q)
11	15.8 (q)	15.6 (q)	16.1 (q)	15.8 (q)	15.8 (q)	15.5 (q)	16.0 (q)	15.6 (q)	11.8/13.2 (q)	11.9/13.2 (q)	8.3 (q)	8.3 (q)			15.9 (q)	15.6 (q)
1′			44.7 (t)	44.9 (t)	81.7 (d)	81.9 (d)	172.0 (s)	171.8 (s)							41.4 (t)	41.6 (t)
2′			59.7 (t)	59.6 (t)	73.4 (d)	73.5 (d)	63.2 (d)	63.2 (d)							25.0 (t)	24.9 (t)
3′					77.1 (d)	77.0 (d)	31.4 (d)	31.2 (d)							31.8 (t)	31.7 (t)
4′					69.8 (d)	69.8 (d)	19.4 (q) [b]	19.5 (q) [b]							173.3 (s)	173.3 (s)
5′					78.8 (d)	78.9 (d)	18.1 (q)	18.1 (q)								
6′					60.9 (t)	60.9 (t)										

[b] Interchangeable; * overlapped by the solvent signal.

Table 3. ^{1}H NMR Spectroscopic Data for Compounds **5–8** in DMSO-d_6.

No.	5a1–2	5b1–2	6a	6b	7a	7b	8a	8b
5			3.60 (1H, br s)	3.69 (1H, br s)	3.40 (1H, dd, 3.0, 0.9)	3.49 (1H, dd, 3.2, 1.0)	3.44 (1H, dd, 3.0, 0.8)	3.54 (1H, dd, 3.2, 0.9)
7	2.30 (3H, s)	2.33 (3H, s)	2.32 (3H, s)	2.34 (3H, s)	2.31 (3H, s)	2.34 (3H, s)	2.45 (3H, s)	2.48 (3H, s)
8	1.68 (1H, m)	1.68 (1H, m)	1.77 (1H, m)	1.77 (1H, m)	1.98 (1H, m)	1.98 (1H, m)	1.72 (1H, m)	1.72 (1H, m)
9	0.85/0.96, 1.15/1.74 (each 1H, m)	0.85/0.96, 1.15/1.74 (each 1H, m)	3.61 (1H, m)	3.61 (1H, m)	0.92 (3H, d, 7.0)	0.92 (3H, d, 7.0)	1.07, 1.22 (each 1H, m)	1.07, 1.22 (each 1H, m)
10	0.76/0.84 (3H, t, 7.1)	0.76/0.84 (3H, t, 7.1)	1.064 (3H, d, 6.2)	1.069 (3H, d, 6.2)			0.79 (3H, t, 7.4)	0.80 (3H, t, 7.4)
11	0.61/0.89 (3H, d, 6.9)	0.62/0.89 (3H, d, 6.9)	0.614 (3H, d, 6.8)	0.607 (3H, d, 6.8)	0.67 (3H, d, 7.0)	0.69 (3H, d, 7.0)	0.89 (3H, d, 7.0)	0.88 (3H, d, 6.9)
1′							3.33 (2H, m)	3.36 (2H, m)
2′							1.74 (2H, m)	1.74 (2H, m)
3′							2.12 (2H, t, 7.3)	2.12 (2H, t, 7.3)
1-NH	7.70/7.77 (1H, s)	7.47/7.55 (1H, s)	7.07 (1H, s)	6.84 (1H, s)	7.54 (1H, s)	7.32 (1H, s)	10.53 (1H, t, 5.9)	10.81 (1H, t, 5.9)
12-NH	8.59, 9.28 (each 1H, br s)	8.71, 9.47 (each 1H, br s)	8.70, 9.44 (each 1H, br s)	8.84, 9.67 (each 1H, br s)	8.66, 9.43 (each 1H, br s)	8.80, 9.67 (each 1H, br s)	6.82, 7.37 (each 1H, br s)	6.82, 7.37 (each 1H, br s)
OH	5.60/5.62 (1H, s)	5.63/5.65 (1H, s)						
CONH							7.62 (1H, br s)	7.35 (1H, br s)

Tenuazamine F (**6**): brown oil droplets; ^{1}H and ^{13}C data, Tables 2 and 3; UV (500 μg/mL, MeOH) λ_{max} 291.0 nm, Figure S42; HRESIMS *m/z* 211.1092 [M−H]$^-$, (calcd. for C$_{11}$H$_{14}$N$_2$O$_4$, 211.1083); $[\alpha]_D^{25}$ −0.6 (*c* 2.0, MeOH).

Tenuazamine G (**7**): brown oil droplets; ^{1}H and ^{13}C data, Tables 2 and 3; UV (500 μg/mL, MeOH) λ_{max} 291.0 nm, Figure S51; HRESIMS *m/z* 183.1116 [M+H]$^+$, (calcd. for C$_9$H$_{15}$N$_3$O$_3$, 183.1133); $[\alpha]_D^{25}$ −8.05 (*c* 2.0, MeOH).

Tenuazamine H (**8**): brown oil droplets; ^{1}H and ^{13}C data, Tables 2 and 3; HRESIMS *m/z* 282.1800 [M+H]$^+$, (calcd. for C$_{14}$H$_{24}$N$_3$O$_3$, 282.1812); $[\alpha]_D^{25}$ 5.1 (*c* 2.0, MeOH).

2.4. Calculation Part

Conformational analyses were conducted through random searches by employing the Sybyl-X 2.0 program using the MMFF94S force field with an energy cutoff of 5 kcal/mol [23]. Results revealed eight low-energy conformers. Subsequently, geometry optimizations and frequency analyses were performed at the B3LYP-D3(BJ)/6-31G* level in CPCM methanol using ORCA5.0.1. [24]. All conformers used for the property calculations in this work were characterized to be stable points on the potential energy surface without any imaginary frequencies. The excitation energies, oscillator strengths, and rotational strengths (velocity) of the first 60 excited states were calculated using the time-dependent density functional theory (TD-DFT) methodology at the PBE0/def 2-TZVP level with CPCM methanol using ORCA5.0.1 [24]. The ECD spectra were simulated using the overlapping Gaussian function (half of the bandwidth was at the 1/e peak height; sigma = 0.30 for all) [25]. Gibbs free energies of conformers were determined via thermal correction at the B3LYP-D3(BJ)/6-31G* level, and electronic energies were evaluated at the wB97M-V/def 2-TZVP level with CPCM methanol using ORCA5.0.1 [24]. To obtain the final spectra, averages of the simulated conformer spectra were calculated according to the Boltzmann distribution theory and their relative Gibbs free energy. The absolute configuration of the only chiral center was determined by comparing the experimentally obtained spectra with the theoretically calculated ones.

### 2.5. Arabidospsis thaliana Phytoxicity Assays

The activity was determined according to the method described by Shi et al. [26]. All experiments were performed on *A. thaliana* leaves of the Columbia-0 ecotype 441 (Col-0) at 3 weeks old and were adapted for 24 h at 22 °C ± 0.5 °C in a growth chamber prior to inoculation. By taking 5 μL of a solution containing compounds **1–9,** glyphosate (dissolved in methanol, 1 mg/mL), and methanol, and dropping it onto the surface of *Arabidopsis* leaves, all leaves in each plant participated in the test. Glyphosate and methanol as positive and negative control groups, respectively, were used to compare the changes in *Arabidopsis* leaves in the experimental group. After adding the medication dropwise, it was placed in a light incubator (22 °C, humidity of 70%, illumination of 2000–3000 lux, photoperiod 14 h/8 h) and observed for 24 h for 7 times.

3. Results

3.1. Structure Elucidation

Compound **1** was obtained as brown oil droplets and had the molecular formula C$_{10}$H$_{16}$N$_2$O$_2$, as determined by the protonated ion peak at *m/z* 197.1290 in the (+)-HRMS(ESI) spectrum ([M+H]$^+$, calcd. 197.1297), accounting for four indices of hydrogen deficiency. The NMR spectrum showed signal pairs with different intensities and the reproducibility for tautomers **1a** and **1b** in HPLC analysis of the rejections of tautomers **1a** or **1b**, respectively (Figures S2 and S7, SI), suggesting tautomerism for compound **1**. To facilitate structural analysis, we preferentially used the NMR signals of the predominant tautomer (**1a**) for the structural elucidation. The ^{1}H NMR spectrum of tautomer **1a** (Table 1) in DMSO-d_6 gave three singlet signals at δ_H 8.64, 9.42 (each 1H for 12-NH$_2$), and δ_H 7.53 (1H for 1-NH), a nitrogen-bearing methine signal resonating at δ_H 3.44 (1H, br d, *J* = 2.9 Hz, H-5), as well as one olefinic methyl at δ_H 2.30 (3H, s, H-7), and two aliphatic methyl signals at δ_H 0.79 (3H,

t, *J* = 7.4 Hz) and 0.88 (3H, d, *J* = 7.0 Hz) in the high-field region (Figure 1). The ^{13}C NMR spectrum showed 10 carbon signals, including signals assigned to two carbonyl groups (C-2, δ_C 174.6 and C-4, δ_C 195.9), two olefinic carbons at δ_C 167.2 (C-6) and 95.4 (C-3), one N-bearing methine at δ_C 64.9 (CH-5), one sp^3 methylene (CH$_2$-9, δ_C 23.0), one sp^3 methine (CH-8, δ_C 36.5), and three methyls (δ_C 18.5, 15.8, 11.9) in the high-field region. Two carbonyl groups and one carbon–carbon double bond occupied three degrees of unsaturation, revealing a monocyclic system in tautomer **1a**. Further analysis of the ^{1}H–^{1}H COSY spectrum revealed the presence of a *sec*-butyl moiety by the correlation systems from H$_3$-10 (δ_H 0.79) to H$_3$-11 (δ_H 0.88) via H$_2$-9 (δ_H 1.08 and 1.23) and H-8 (δ_H 1.72) (Figure 2). The aforementioned NMR data indicated tautomer **1a** to be a structural analog of TeA (**9**), with the differences being the 3-NH$_2$ substituted α, β-unsaturated keto in tautomer **1a** rather than the corresponding 1-OH substituted α, β-unsaturated keto in the head-to-tail transposition position [26,27]. This was further verified through HMBC analysis, especially by the cross-peaks from H$_3$-7 (δ_H 2.30) to C-3 (δ_C 95.4) and C-6 (δ_C 167.2) and H-1 (δ_H 7.53) to C-3 and C-4 (δ_C 195.9) (Figure 2). The loose end of C-6 was confirmed to be the 6-NH$_2$ group by the chemical shifts for C-3 and C-6 due to the electron-donating inductive effect of the remaining amino group. This was reasonably in accordance with the elementary composition for tautomer **1a**. The relative configurations of the carbon centers for tautomer **1** were proposed as depicted on the basis of chemical evidence and biogenetic considerations which were consistent with those of tenuazonic acid with a $\Delta\delta_C$ value within 0.9–1.6 ppm, especially the stereo centers of C-5 ($\Delta\delta_C$ 0.9–1.4 ppm) and C-8 ($\Delta\delta_C$ 1.1–1.6 ppm) [28]. The minor tautomer (**1b**) was ascribed to be the same gross structure as that of tautomer **1a** by the compressive assignments of the NMR data, especially the scrutiny of the 2D NMR data of tautomer **1b,** and the spectra were examined for evidence of minor tautomer and assigned their peaks, where possible (Table 1). Compared to the major tautomer **1a**, the intramolecular hydrogens bond formation for **1b** between 12-NH$_2$ with C-4 rather than between 12-NH$_2$ with C-2 were confirmed by the down-fielded shifts for C-4 ($\Delta\delta_C$ +1.6 ppm) and up-fielded shifts for C-2 ($\Delta\delta_C$ −2.5 ppm) [27,28], suggesting the *Z/E* isomerism for carbon–carbon double bonds between the predominant tautomer (**1a**) and the minor one (**1b**). To determine the absolute configuration of compound **1**, we calculated the ECD spectra of tautomers **1a** and **1b** as the same ratio of 10:7 (same as identified by ^{1}H NMR data) using TD-DFT at the B3LYP D3(BJ)/6-31G level with the CPCM model [24]. Fortunately, the calculated spectra of **1** 5*S*, 8*S*, *Z* (**1a**) and 5*S*, 8*S*, *E* (**1b**) = 10:7 were in good agreement with the corresponding experimental spectrum of compound **1** (Figure 3). Thus, the structure of compound **1** was established, as shown in Figure 1, and named tenuazamine A.
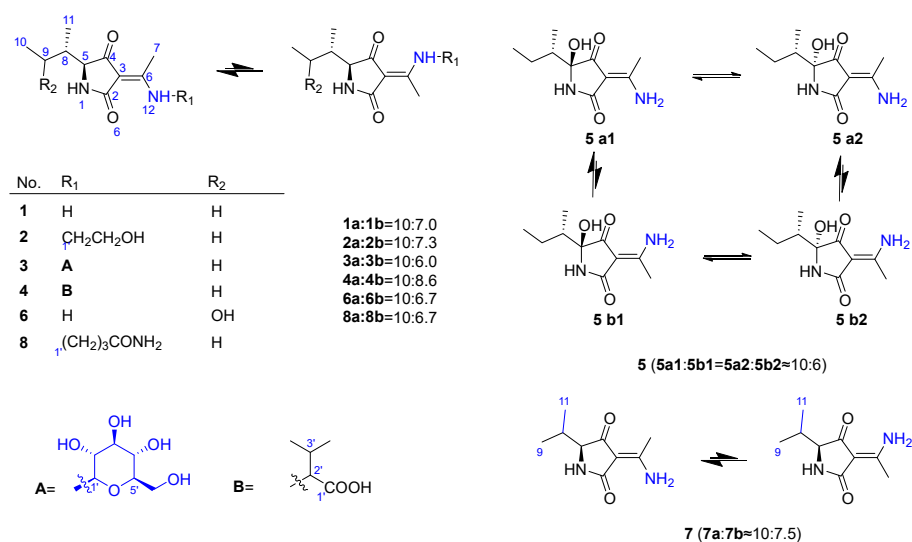
Figure 1. Chemical structures of **1**–**8** derived from *A. alternata* FL7.

— ¹H-¹H COSY   ⌒ HMBC
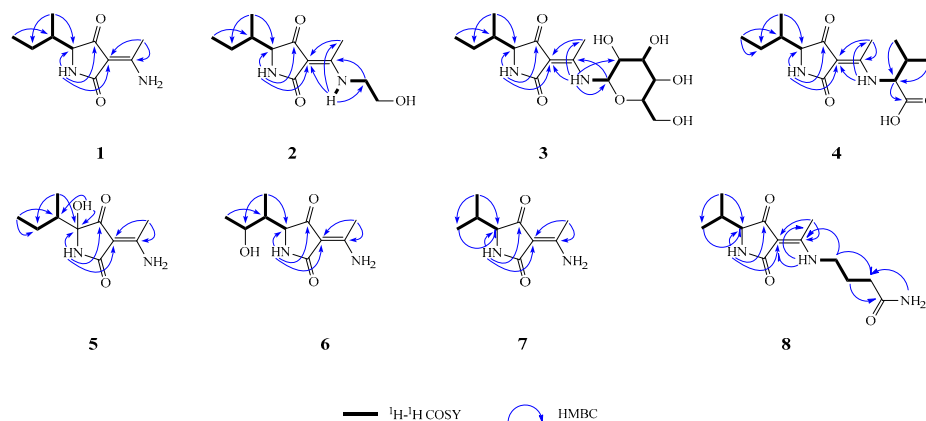
Figure 2. The key COSY (bond lines) and HMBC (blue arrows) correlations of compounds **1–8**.
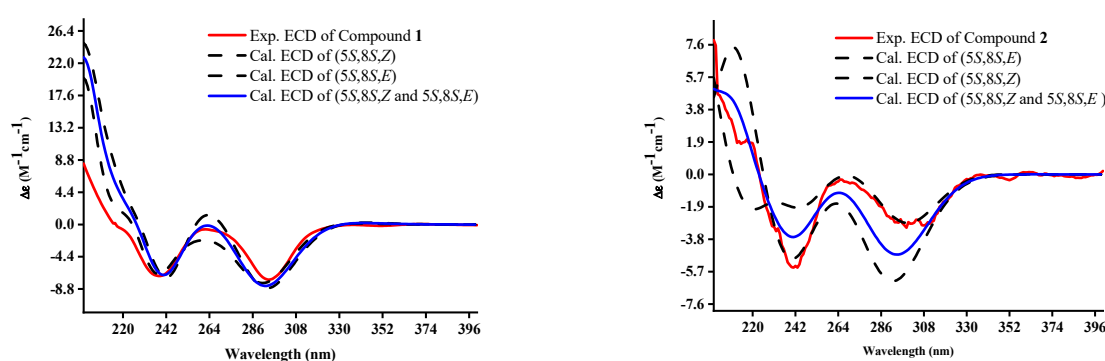
Figure 3. Experimental and calculated ECD spectra of compounds **1–2**.

Compound **2** was also obtained as brown oil droplets and had the molecular formula $C_{12}H_{20}N_2O_3$, as indicated by the positive ion peak at *m/z* 263.1359 in the (+)-HRMS(ESI) spectrum ([M+Na]⁺, calcd. 263.1372). The ¹H and ¹³C NMR spectra of tautomer **2a** resembled these of the predominant tautomer **1a** in compound **1** (Tables 1 and 2), with the major differences being the presence of the two additional methylene signals at δ_C 59.7 (t, C-14) and 44.7 (t, C-13). Considering the molecular formula of **2a**, a hydroxyethyl group has to be substituted on the amino group of C-6. Hence, the resulting structure was further verified using detailed ¹H–¹H COSY correlations between H-1′ (δ_H 3.40) and NH-12 (δ_H 10.58), together with the cross-peaks from H₂-1′ to C-6 (δ_C 167.9), and NH-12 to C-1′ (δ_C 44.7) in the HMBC spectrum (Figure 2), and the up-fielded shift for CH₃-7 (δ_C −4.6 ppm) in ¹³C NMR data. Similar to compound **1**, the *Z/E* isomerism of carbon–carbon double bonds between the predominant tautomer (**2a**) and the minor one (**2b**) in compound **2**, was confirmed by the down-fielded shifts for C-4 ($\Delta\delta_C$ +2.8 ppm) and up-fielded shifts for C-2 ($\Delta\delta_C$ −2.9 ppm) for **2b**, [28] due to the intramolecular hydrogens bond formation for **2b** between 12-NH with C-4 rather than between 12-NH with C-2. The relative configurations of compound **2** were consistent with those of **1**, as determined by a comparison of the NMR shifts of the *sec*-butyl moieties, especially the ¹³C NMR data of the center carbons C-5 ($\Delta\delta_C$ −0.3 ppm) and C-8 ($\Delta\delta_C$ +0.2 ppm) and biogenetic considerations. The absolute configurations of **2** were assigned as (5*S*, 8*S*, *Z* for **2a** and 5*S*, 8*S*, *E* for **2b**) by comparing its experimental and calculated ECD spectra (Figure 3). Therefore, the structure of compound **2** was established, as shown in Figure 1, and it was named tenuazamine B.

Compound **3** was also obtained as brown oil droplets and had the molecular formula $C_{16}H_{26}N_2O_7$, as gleaned from the sodiated molecular ion peak at *m/z* 381.1633 in the (+)-HRMS(ESI) analysis ([M+Na]⁺, calcd. 381.1638), with one more degree of unsaturation than compound **1**. The NMR data of six additional oxygenated ones (five methines and one methylene) in compound **3** indicated that it was a glycoside derivative of **1**, and the NMR signals of the notable tautomer (**3a**) were used for the subsequent structural

interpretation. Except for six additional oxygenated carbons (δ_C 81.7, 78.8, 77.1, 73.4, 69.8, 60.9), the 1D NMR data (Tables 1 and 2) of **3a** exhibited similarities to those of **1a**, suggesting the structural resemblance between **3a** and **1a**. Besides the difference at C-7 ($\Delta\delta_C$ −5.0 ppm), all other carbons with almost identical chemical shifts ($\Delta\delta_C$ 0.0–0.5 ppm), that suggested the glycoside appendage was attached to the 12-amino group via the anomeric C-1' (δ_C 81.7) in **3a**. This structural deduction was confirmed by careful interpretation of the 2D NMR data, especially, the HMBC correlations from H-1' (δ_H 4.69) to C-6 (δ_C 167.7) and from NH-12 (δ_H 10.73) to C-1' (δ_C 81.7) and C-2' (δ_C 73.4) (Figure 2), as well as the ^{1}H–^{1}H COSY correlation systems from N-12 to H$_2$-6' (Figure 2). The relative configuration of the aglycone unit in **3a** was deduced to be consistent with that of **1a** by comparing the NMR shifts of the stereocenters with almost the same chemical carbon shift values for C-5, C-8, C-9, C-10, and C-11 for **1a** and **3a**. Furthermore, the relative configuration of the 1-amino-1-deoxy-β-D-glucose was ascribed by the multiplicities of the coupling constants for $J_{1',2'}$, $J_{2',3'}$, $J_{3',4'}$, $J_{4',5'}$ with about 9.0 Hz, which was supported by biogenetic considerations. Similar to compound **1**, the *Z/E* isomerism of carbon–carbon double bonds between the predominant tautomer (**3a**) and the minor one (**3b**) in compound **3**, based on the down-fielded shifts for C-4 (δ_C +2.8 ppm) and up-fielded shifts for C-2 (δ_C −3.1 ppm) for **3b** [28] due to the intramolecular hydrogens bond formation for **3b** between 12-NH with the keto carbonyl (C-4) rather than between 12-NH with the amidocarbonyl group (C-2). Finally, the chemical structure of the new *N*-glycoside was established, and it was named tenuazamine C.

Compound **4** was obtained as brown oil droplets and had the molecular formula $C_{15}H_{24}N_2O_4$, as indicated by the *quasi*-molecular ion peak of *m/z* 297.1802 in the (+)-HRMS(ESI) spectrum (calcd. 297.1814), accounting for five degrees of unsaturation. The ^{13}C NMR spectrum (Table Table 1 and Table Table 2) included 15 carbon signals, with 10 being considerably similar to those of tenuazamine A (**1**), indicating that it was a structural congener of compound **1**. The noticeable difference was the presence of five additional carbon signals, one carbonyl (δ_C 172.0), two methines (δ_C 63.2 and 31.4), and two methyls (δ_C 19.4 and 18.1) in **4**. Considering the molecular formula and through the analysis of the obtained 2D NMR spectra (Figure 2), the new signals were assigned to a 3-methylbutanoic acid moiety using the HMBC correlations from H-2' (δ_H 3.76) to C-1' (δ_C 172.0) and the cross-peaks between H-3' (δ_H 2.15) and H$_3$-4' (δ_H 0.86) and H$_3$-5' (δ_H 0.91) in the ^{1}H–^{1}H-COSY spectrum of the major tautomer **4a**. Furthermore, the ^{1}H–^{1}H-COSY correlation (Figure 1) between 12-NH and H-2' revealed the association of the 3-methylbutanoic acid moiety, to be a five-carbon adduct of the 12-NH. Similar to compound **1**, the *Z/E* isomerism of carbon–carbon double bonds between the predominant tautomer (**4a**) and the minor one (**4b**) in compound **4**, was confirmed by the down-fielded shifts for C-4 (+2.8 ppm) and up-fielded shifts for C-2 (−2.8 ppm) for **4b** [28] due to the intramolecular hydrogens bond formation for **4b** between 12-NH with keto group (C-4) rather than between 12-NH with acylamino (C-2). Finally, the chemical structure of the new compound was established, as shown in Figure 1, and it was named tenuazamine D.

Compound **5** was obtained as brown oil droplets and had the molecular formula of $C_{10}H_{16}N_2O_3$, as indicated by the negative *quasi*-molecular ion peak at *m/z* 211.1092 [M−H]$^-$ (calcd. 211.1083) in (−)-HRMS(ESI). Its 1D NMR data (Tables 2 and 3) were highly similar to those of **1**, but with the absence of the proton signal of CH-5 (δ_H 3.44/3.53 and δ_C 64.9/63.6 for **1a** and **1b**), and in the concomitant presence of non-hydrogen bearing carbon resonances (δ_C 87.85/87.87 for **5a1** and **5a2**, 87.02/87.03 for **5b1** and **5b2**, respectively), suggesting the existence of a new substituent at C-5, which was then identified as hydroxyl groups by ESIMS and HMBC spectra (Figure 2). Specifically, the HMBC correlations (Figure 2) from the 1-NH signals at δ_H 7.70/7.77 (1H, s, 1-NH), 5.60/5.62 (1H, s, 5-OH), and 0.61/0.89 (3H, d, *J* = 6.9 Hz, H$_3$-11) to the non-oxygenated bearing C-5 (δ_C 87.9) confirmed that the hydroxyl groups were substituted at C-5 for tautomers **5a1** and **5a2**. Given the hemiketal property of the hydroxyl group, the configurations of C-5 were rapidly isomerized, and the isomers existed in the solution in nearly equal quantities. As compared with those

of **1a**, the relative *α*-configurations for 5-OHs of tautomers **5a2** and **5b2** were assigned by the up-fielded ^{13}C NMR data for C-8, C-9, and C-11 with more values of $\Delta\delta_C$ −1.5, and −4.0 ppm by the *γ*-gauche effects resulting from the 5*α*-OHs. Consequently, the 5-OHs of tautomers **5a1** and **5b1** were *β*-oriented with less values of $\Delta\delta_C$ −2.6 ppm for C-11, even down-fielded shift for C-9 ($\Delta\delta_C$ +0.3 ppm) resulting in less repulsion of 5-NHs. Similar to compound **1**, the *Z/E* isomerism of carbon–carbon double bonds between the predominant tautomers (**5a1** and **5a2**) and the minor ones (**5b1** and **5b2**) in compound **5** was verified by the down-fielded shifts for C-4 ($\Delta\delta_C$ +2.3 ppm) and up-fielded shifts for C-2 ($\Delta\delta_C$ −2.7 ppm) for **5b1** and **5b2**. This was due to the intramolecular hydrogen bond formation for **5b1** and **5b2** between 12-NH with keto functional groups (C-4) rather than between 12-NH with amide carbonyls (C-2). Thus, the chemical structure of the new compound was established, as shown in Figure 1, and it was named tenuazamine E.

Compound **6** was obtained as brown oil droplets and had the molecular formula $C_{10}H_{16}N_2O_3$, as indicated by the negative HR-ESI–MS (*m/z* based on [M−H]$^-$: 211.1092; calcd. 211.1083), suggesting to be an oxygenated derivative of compound **1**. The ^{13}C NMR spectrum (Table 2) of the major tautomer **6a** shows 10 carbon signals being considerably similar to those of the tautomer **1a** of tenuazamine A (**1**), being the absence of a methene (δ_H 1.08, 1.23, and δ_C 23.0) and the concomitant presence of an oxygen-bearing methine (δ_H 3.61 and δ_C 68.5) in compound **6a**, as well as the down-field chemical shifts of CH$_3$-10 ($\Delta\delta_H$ +0.27 ppm and $\Delta\delta_C$ +9.6 ppm) and CH-8 (δ_H +0.05 ppm and δ_C +4.8 ppm) by the inductive effect of hydroxyl group and up-field chemical shifts for CH$_3$-11 ($\Delta\delta_H$ −0.27 ppm and $\Delta\delta_C$ −7.5 ppm) due to the *γ*-gauche effect between CH$_3$-11 and 9-OH. The structural assignment of **6a** was confirmed by the interpretation of its 2D NMR data, especially the HMBC cross-peaks from H$_3$-11 (δ_H 0.61) to CH-9 (δ_C 68.5) and the spin-coupling systems from H-8 (δ_H 1.77) to H$_3$-11 (δ_H 0.61), and from H-5 (δ_H 3.60) to H$_3$-10 (δ_H 1.06) via H-9 (δ_H 3.61) ascribed from the ^{1}H-^{1}H COSY spectrum. Similar to compound **1**, the *Z/E* isomerism of carbon–carbon double bonds between the predominant tautomer (**6a**) and the minor one (**6b**) in compound **6** was verified by the down-fielded shifts for C-4 ($\Delta\delta_C$ +2.6 ppm) and up-fielded shifts for C-2 ($\Delta\delta_C$ −2.5 ppm) for **6b**, due to the intramolecular hydrogens bond formation for **6b** between 12-NH with keto functional groups (C-4) rather than between 12-NH with amide carbonyls (C-2). Finally, the chemical structure of the new compound **6** was established (Figure 1), and it was named tenuazamine F.

Compound **7** was obtained as brown oil droplets and had the molecular formula $C_9H_{14}N_2O_2$, as indicated by positive HR-ESI–MS (*m/z* based on [M+H]$^+$: 183.1116; calcd. 183.1133), with less CH$_2$ moiety than compound **1**. The ^{1}H and ^{13}C NMR spectra of the major tautomer **7a** resembled those of tautomer **1a** (Tables 2 and 3), with the major differences being one less methene signal and the presence of a doublet methyl group (CH$_3$-9, δ_C 19.5, δ_H 0.92) in **7a** instead of the corresponding triplet methyl moiety (CH$_3$-10, δ_C 11.9, δ_H 0.79) in **1a**. This structural deduction was confirmed by the 2D NMR data, especially by the HMBC correlations from H$_3$-11 (δ_H 0.67) to CH$_3$-9 (δ_C 19.5) and C-5 (δ_C 65.1), as well as the spin-coupling systems from H-8 to H$_3$-9 and H$_3$-11 assigned by the ^{1}H-^{1}H COSY spectrum. Similar to compound **1**, the *Z/E* isomerism of carbon–carbon double bonds between the predominant tautomer (**7a**) and the minor one (**7b**) in compound **7** was verified by the down-fielded shifts for C-4 ($\Delta\delta_C$ +2.6 ppm) and up-fielded shifts for C-2 ($\Delta\delta_C$ −2.5 ppm) for **7b**,[19] due to the intramolecular hydrogens bond formation for **7b** between 12-NH with keto functional groups (C-4) rather than between 12-NH with amide carbonyls (C-2). Finally, the chemical structure of compound **7** was established, as shown in Figure 1, and it was named tenuazamine G.

Compound **8** was a white amorphous powder and had the molecular formula of $C_{14}H_{23}N_3O_3$, as indicated by the positive HR-ESI–MS (*m/z* [M+H]$^+$: 282.1800, calcd. 282.1812), accounting for five degrees of unsaturation. The ^{1}H and ^{13}C NMR spectra of major tautomer **8a** resembled these of the predominant tautomer **1a** in compound **1** (Tables 2 and 3), with the major differences being the presence of the four extra carbon signals for one amido-carbonyl carbon (δ_C 173.3) and three aliphatic methylene carbons

(δ_C 41.4, 31.8, and 25.0) in **8a**. Considering the elementary composition of **8a**, 4-butyramide moiety has to be substituted on the 12-NH group. Hence, the resulting structure was further verified using detailed ^{1}H–^{1}H COSY correlations from 3'-CH$_2$ (δ_H 1.74) to 12-NH (δ_H 10.53), together with the cross-peaks from H$_2$-1' (δ_H 3.33) to C-6 (δ_C 167.3), and H$_2$-2' (δ_H 1.74) to C-4' (δ_C 173.3), and 4'-NH$_2$ (δ_H 6.82, 7.37) to CH$_2$-3' (δ_C 31.8) in the HMBC spectrum (Figure 2). Similar to compound **1**, the *Z/E* isomerism of carbon–carbon double bonds between the predominant tautomer (**8a**) and the minor one (**8b**) in compound **8**, was confirmed by the down-fielded shifts for C-4 ($\Delta\delta_C$ +3.1 ppm) and up-fielded shifts for C-2 ($\Delta\delta_C$ −3.3 ppm) for **8b**, due to the intramolecular hydrogens bond formation for **8b** between 12-NH with keto carbonyl rather than between 12-NH with amide carbonyl. The relative configurations of compound **8** were consistent with those of **1**, as determined by a comparison of the NMR shifts of the *sec*-butyl moieties, especially the ^{13}C NMR data of the center carbons C-5 ($\Delta\delta_C$ +0.04 ppm) and C-8 ($\Delta\delta_C$ −0.03 ppm) and biogenetic considerations. Finally, the structure of **8** was established, as shown in Figure 1. and it was named tenuazamine H.

3.2. Biological Activity of the Compounds on A. thaliana

The activity results indicate that all tested substances (**1**–**9**) displayed varying levels of phytotoxicity, as depicted in Figure 4. Evaluate the effects of various compounds on Arabidopsis growth by observing plant height, leaf quantity, color, and spots. Notably, the blank control group of *A. thaliana* did not receive any impact. Tenuazamine A (**1**), tenuazamine D (**4**), tenuazamine H (**8**), TeA (**9**), and the positive control (glyphosate) also exhibited obvious toxicity in the leaves of *A. thaliana* because they noticeably turned yellow (Figure 4). In addition, the *Arabidopsis* plants tested for the above compounds did not show significant changes in plant height, spots, or quantity, except for leaf chlorosis. Shi et al. uncovered that TeA toxin-induced photosynthetically generated 1O$_2$ in *A. thaliana* triggers EXECUTER1 (EX1)/EX2-mediated chloroplast-to-nucleus retrograde signaling (RS), ultimately leading to the demise of *A. thaliana* leaves [29]. As depicted in Figure 4, Compared to compound **1**, the decrease in activity observed in compounds **2**–**3** and **5**–**7** could be attributed to the varying substitutions on the 12-NH$_2$ moiety, but the butanamide substituted congener **8** with more potent activity indicated the butanamide group played a key role to the herbicidal activity. The tested compounds with hydroxyl groups on the core skeletons, such as hydroxyls on C-5 (**5**) and C-9 (**6**), were nearly inactive. Furthermore, compound **7** with one carbon less showed less toxicity and indicated the more compact carbon skeleton attenuated the herbicidal activity. This phenomenon may be linked to the attenuation strategies adopted by pathogenic fungi transitioning into endophytic fungi, as they adapt to the less hostile plant endosphere environment.
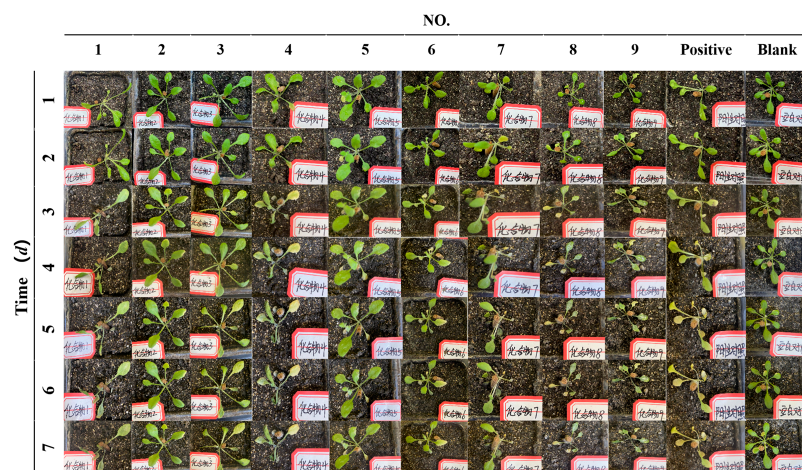
Figure 4. Toxicity of compounds **1**–**9** to *Arabidopsis thaliana*. (Note. the Chinese characters in the picture means "compound").

4. Conclusions

These results considerably enrich the secondary metabolite library of *A. alternata* and provide a series of new compounds with potentially phytotoxic activity on *Arabidopsis thaliana*. Meanwhile, they may have the potential for further research as biological herbicides, providing reference value for the secondary metabolites of fungi in agricultural weed control work.

References

1. Lou, J.F.; Fu, L.Y.; Peng, Y.L.; Zhou, L.G. Metabolites from *Alternaria* Fungi and Their Bioactivities. *Molecules* **2013**, *18*, 5891–5935. [CrossRef]
2. Ceci, A.; Pinzari, F.; Russo, F.; Maggi, O.; Persiani, A.M. Saprotrophic soil fungi to improve phosphorus solubilisation and release: In vitro abilities of several species. *Ambio* **2018**, *47*, 30–40. [CrossRef]
3. Shi, Z.Z.; Miao, F.P.; Fang, S.T.; Liu, X.H.; Yin, X.L.; Ji, N.Y. Sesteralterin and tricycloalterfurenes A–D: Terpenes with rarely occurring frameworks from the marine-alga-epiphytic fungus *Alternaria alternata* k21-1. *J. Nat. Prod.* **2017**, *80*, 2524–2529. [CrossRef]
4. Gabriel, M.F.; Postigo, I.; Tomaz, C.T.; Martínez, J. *Alternaria alternata* allergens: Markers of exposure, phylogeny and risk of fungi induced respiratory allergy. *Environ. Int.* **2016**, *89*, 71–80. [CrossRef] [PubMed]
5. Paschapur, A.U.; Subbanna, A.R.N.S.; Singh, A.K.; Jeevan, B.; Stanley, J.; Rajashe-kara, H.; Pattanayak, A. *Alternaria alternata* strain VLH1: A potential entomopathogenic fungus native to North Western Indian Himalayas. *Egypt. J. Biol. Pest Control* **2022**, *32*, 138. [CrossRef]
6. Nagda, A.; Meena, M. *Alternaria* mycotoxins in food and feed: Occurrence, biosynthesis, toxicity, analytical methods, control and detoxification strategies. *Food Control* **2023**, *158*, 110211. [CrossRef]
7. Zhang, Y.; Liao, G.; Wang, M.; Zhang, Z.; Liu, L.; Song, Y.; Chen, Y. Human-associated bacteria adopt an unusual route for synthesizing 3-acetylated tetramates for environmental adaptation. *Microbiome* **2023**, *11*, 97. [CrossRef]
8. Rosett, T.; Sankhala, R.H.; Stickings, C.E.; Taylor, M.E.U.; Thomas, R. Studies in the biochemistry of micro organisms. 103. Metabolites of *Alternaria tenuis* Auct.: Culture filtrate products. *Biochem. J.* **1957**, *67*, 390. [CrossRef]
9. Shi, J.; Zhang, M.; Gao, L.; Yang, Q.; Kalaji, H.M.; Qiang, S.; Chen, S. Tenuazonic acid triggered cell death is the essential prerequisite for *Alternaria alternata* (Fr.) Keissler to infect successfully host *Ageratina adenophora*. *Cells* **2021**, *10*, 1010. [CrossRef]
10. Bjørk, P.K.; Rasmussen, S.A.; Gjetting, S.K.; Havshøi, N.W.; Petersen, T.I.; Ipsen, J.Ø.; Fuglsang, A.T. Tenuazonic acid from *Stemphylium loti* inhibits the plant plasma membrane H+ATPase by a mechanism involving the C-terminal regulatory domain. *New Phytol.* **2020**, *226*, 770–784. [CrossRef] [PubMed]
11. Oliveira, R.C.; Carnielli, Q.L.; Correa, B. *Epicoccum sorghinum* in food: Occurrence, genetic aspects and tenuazonic acid production. *Curr. Opin. Food Sci.* **2018**, *23*, 44–48. [CrossRef]
12. Shigeura, H.T.; Gordon, C.N. The biological activity of tenuazonic acid. *Biochem. J.* **1963**, *2*, 1132–1137. [CrossRef] [PubMed]

13. Chatterjee, S.; Ghosh, R.; Mandal, N.C. Production of bioactive compounds with bactericidal and antioxidant potential by endophytic fungus *Alternaria alternata* AE1 isolated from *Azadirachta indica* A. *Juss. PLoS ONE* **2019**, *14*, e0214744. [CrossRef] [PubMed]

14. Zorofchian Moghadamtousi, S.; Nikzad, S.; Abdul Kadir, H.; Abubakar, S.; Zandi, K. Potential antiviral agents from marine fungi: An overview. *Mar. Drugs* **2015**, *13*, 4520–4538. [CrossRef] [PubMed]

15. Lang, G.; Blunt, J.W.; Cummings, N.J.; Cole, A.L.; Munro, M.H. Paecilosetin, a New Bioactive Fungal Metabolite from a New Zealand Isolate of *Paecilomycesf arinosus*. *J. Nat. Prod.* **2005**, *68*, 810–811. [CrossRef]

16. Hellwig, V.; Grothe, T.; Mayer Bartschmid, A.N.K.E.; Endermann, R.; Geschke, F.U.; Henkel, T.; Stadler, M. *Altersetin*, a new antibiotic from cultures of endophytic *Alternaria* spp. *Taxonomy*, *fermentation*, isolation, structure elucidation and biological activities. *J. Antibiot.* **2002**, *55*, 881–892. [CrossRef]

17. Mao, Z.; Wang, W.; Su, R.; Gu, G.; Liu, Z.L.; Lai, D.; Zhou, L. Hyalodendrins A and B, new decalin type tetramic acid larvicides from the endophytic fungus *Hyalodendriella* sp. Ponipodef 12. *Molecules* **2019**, *25*, 114. [CrossRef]

18. Marfori, E.C.; Kajiyama, S.I.; Fukusaki, E.I.; Kobayashi, A. Phytotoxicity of the tetramic acid metabolite trichosetin. *Phytochemistry* **2023**, *62*, 715–721. [CrossRef]

19. Abdou, R.; Dawoud, M. Cytotoxic Metabolites Of Alternaria Alternata, An Endophyte Of The Medicinal Plant Bidens Bipinnata. *Int. J. Pharm. Pharm. Sci.* **2020**, *12*, 42–48. [CrossRef]

20. Wang, Y.; Lai, Z.; Li, X.X. Isolation, diversity and acetylcholinesterase inhibitory activity of the culturable endophytic fungi harboured in *Huperzia serrata* from Lushan Mountain, China. *World J. Microbiol. Biotechnol.* **2016**, *32*, 20. [CrossRef]

21. Vu, D.; Groenewald, M.; Vries, M.; Gehrmann, T.; Stielow, B.; Eberhardt, U.; Al-Hatmi, A.; Groenewald, J.Z.; Cardinali, G.; Houbraken, J.; et al. Large-scale generation and analysis of filamentous fungal DNA barcodes boosts coverage for kingdom fungi and reveals thresholds for fungal species and higher taxon delimitation. *Stud. Mycol.* **2019**, *20*, 135–154. [CrossRef] [PubMed]

22. White, T.J.; Bruns, T.; Lee, S.; Taylor, J. Amplification and direct sequencing of fungal ribosomal RNA genes for phylogenetics. *PCR Protoc. A Guide Methods Appl.* **1990**, *18*, 315–322.

23. *Sybyl Software*, Version X 2.0; Tripos Associates Inc.: St. Louis, MO, USA, 2013.

24. Neese, F. The ORCA program system, Wiley Interdiscip. *Rev. Comput. Mol. Sci.* **2012**, *2*, 73–78. [CrossRef]

25. Stephens, P.J.; Harada, N. ECD cotton effect approximated by the Gaussian curve and other methods. *Chirality* **2010**, *22*, 229–233. [CrossRef]

26. Shi, J.; Wang, H.; Li, M.; Mi, L.; Gao, Y.; Qiang, S.; Chen, S. *Alternaria* TeA toxin activates a chloroplast retrograde signaling pathway to facilitate JA dependent pathogenicity. *Plant Commun.* **2024**, *5*, 100775. [CrossRef] [PubMed]

27. Gallardo, G.L.; Peña, N.I.; Chacana, P.; Terzolo, H.R.; Cabrera, G.M. L-Tenuazonic acid, a new inhibitor of *Paenibacillus* larvae. *World J. Microb. Biot.* **2004**, *20*, 609–612. [CrossRef]

28. Mikula, H.; Horkel, E.; Hans, P.; Hametner, C.; Fröhlich, J. Structure and tautomerism of tenuazonic acid a synergetic computational and spectroscopic approach. *J. Hazard. Mater.* **2013**, *250*, 308–317. [CrossRef]

29. Yun, C.S.; Motoyama, T.; Osada, H. Regulatory mechanism of mycotoxin tenuazonic acid production in *Pyricularia oryzae*. *ACS Chem. Biol.* **2017**, *12*, 2270–2274. [CrossRef]